Master′s Thesis

Distribution of dissolved inorganic radiocarbon in the Amundsen Sea, Antarctica

남극 아문젠해 용존무기탄소의 방사성탄소 분포

August 2016

Graduate School

Seoul National University

Earth and Environmental Sciences

KIM, BUMSOO

ABSTRACT

The Amundsen Sea is experiencing rapid change in sea-ice cover and ice shelf melting. It has the most productive polynya, the Amundsen Sea polynya. However, the inorganic carbon cycling associated with this polynya is yet poorly determined. In this study, I have examined the distribution of dissolved inorganic radiocarbon (DIC) in three different oceanographic regions in the Amundsen Sea: in the sea-ice zone (SIZ), inside the Amundsen Sea polynya, and near the Dotson Ice Shelf. In the upper 300 m layers, the average radiocarbon value in $\Delta^{14}C$ in the polynya (−135 ‰) was considerably higher than that in the SIZ (−150 ‰). $\Delta^{14}C$ value of Winter Water (WW) end-member was −147 ‰. The $\Delta^{14}C$ values near the sea floor at each site were close to the value of the Circumpolar Deep Water (CDW), reflecting the intrusion of this water mass to the shelf near the sea floor. Contribution of carbon from processes such as glacial meltwater (GMW) input, benthic efflux, and remineralization of sinking organic particles in the water column was negligible to change the radiocarbon values of DIC in the water column. Air-sea gas exchange appears to be the primary process to increase radiocarbon content in the upper layer. Based on the observed discrepancy in $\Delta^{14}C$ value between the

SIZ and the polynya, absorption of atmospheric CO_2 during the polynya opening in the austral summer was estimated. This study provides the preliminary data to understand the inorganic carbon cycling in this climate-sensitive region.

Keywords : dissolved inorganic carbon, radiocarbon, the Amundsen Sea, polynya, air-sea gas exchange

Student Number : 2014-22420

TABLE OF CONTENTS

LIST OF FIGURES

LIST OF TABLES

1. INTRODUCTION

1.1 Dissolved Inorganic Radiocarbon

Dissolved inorganic carbon (DIC) is the largest (~36,000 Gt C) and exchangeable carbon reservoir in the ocean (McNichol et al., 1994; Druffel et al., 2008). DIC represents the total concentration of dissolved inorganic carbon species: bicarbonate ion [HCO_3^-], carbonate ion [CO_3^{2-}], and dissolved carbon dioxide [CO_2]. In the oceanic water column, DIC is consumed by biological production in the surface ocean, and replenished by remineralization of sinking organic matter at depth. As a result, the concentration of DIC is generally depleted in the surface ocean, increases exponentially with depths and remains enriched in the deep ocean. In the global ocean, DIC concentration range from ~2000 to ~2300 μmol/kg (Key et al., 2004). In general, DIC is controlled by physical processes (e.g. mixing, diffusion and air-sea CO_2 exchange) and biological processes (e.g. photosynthesis, respiration and $CaCO_3$ precipitation/dissociation) (Sarmiento and Gruber, 2006; Shadwick et al., 2011).

In the ocean, dissolved inorganic radiocarbon ($DI^{14}C$), radiocarbon content of DIC, can be used as an indicator to determine the water mass transport, to trace the source of carbon and to interpret the interaction with

organic carbon cycling. Radiocarbon (^{14}C) is a radioactive carbon isotope, mainly produced naturally in the atmosphere by cosmic ray (Libby, 1955). The atmospheric ^{14}C reacts with O_2 to form $^{14}CO_2$, and becomes incorporated into the global carbon cycling through the same physical, chemical and biological processes of CO_2. In the ocean, ^{14}C is transferred from the atmosphere by air-sea gas exchange of $^{14}CO_2$. With its half-life of 5730 years and recent rapid change in concentration by thermonuclear bomb test, ^{14}C has been used as an important tracer as a "natural clock" in the marine carbon cycle. World Ocean Circulation Experiment (WOCE) and Geochemical Ocean Section Study (GEOSECS) are one of the renowned expeditions to map the global radiocarbon distribution (Stuiver et al., 1983; Key, 1996). Radiocarbon of DIC has been studied to determine the CO_2 transfer from atmosphere into ocean (Broecker and Peng, 1982); to evaluate the circulation rate between the major deep oceans (Stuiver and Ostlund, 1983; Matsumoto, 2007); to trace the water mass transport including bottom water formation (Weiss et al, 1979; Smethie et al., 1986; Leboucher et al., 1999; Key and McNichol, 2012); to address the interaction between organic carbon cycling in temporal and spatial variability (Bauer et al., 1998; Griffith et al, 2012; Bertrand et al., 2013).

1.2 Radiocarbon Values in the Southern Ocean

Radiocarbon values ($\Delta^{14}C$) are the deviation of $^{14}C/^{12}C$ ratio of sample relative to standard reference ratio after correcting the isotopic fractionation ($\delta^{13}C = -25$ ‰) (Stuiver and Polach, 1977). $\Delta^{14}C$ values of the Southern Ocean are significantly depleted compared to the major oceans, indicating a radiocarbon age of ~1400 yrs in the surface ocean (Key et al., 2004). There are two main reasons for this feature:

(1) Short surface water residence time; It takes nearly 10 years for surface water to become carbon isotopic equilibrium with the atmosphere (Broecker and Peng, 1982). Residence time of surface water is typically shorter than the equilibrium time, causing radiocarbon disequilibrium inferred as the "surface reservoir effect" (Matsumoto, 2007). Thus, surface water residence time influences the radiocarbon input from the atmosphere and consequently affects the surface distribution of radiocarbon. Surface water of the Southern Ocean has a much shorter residence time due to rapid vertical mixing with deep water, implying more depleted radiocarbon signature compared to other major oceans.

(2) Upwelling of Circumpolar Deep Water (CDW); Originated from the strong eastward Antarctic Circumpolar Current, CDW is a relatively warm, saline and dense water mass that circulates around Antarctica within 500 to

1500 m depth. CDW has a radiocarbon value (as in $\Delta^{14}C$) of ~ −160 ‰ (Stuiver et al., 1983; Leboucher et al., 1999; Key and McNichol, 2012) which is the most depleted or "oldest" water mass in the Southern Ocean. Surface $\Delta^{14}C$ measurements show a distinctive contrast across the Polar Front (PF) where upwelling of "old" CDW occurs (Leboucher et al., 1999): enriched (up to ~55 ‰) to the north of PF, and depleted (−140 to −70 ‰) in the upper 200 m depth to the south of PF. Between PF and the Antarctica, $\Delta^{14}C$ values of surface water are more depleted due to the influence of ^{14}C-depeleted CDW and rapid vertical mixing.

1.3 The Amundsen Sea

The Southern Ocean (south of 50 °S) is considered to be an important sink of atmospheric CO_2, despite its small spatial area compared to the major oceans (Takahashi et al., 2009). Antarctica is surrounded by sea-ice perennially. However, polynyas that occur in the Antarctic coast potentially influence the global carbon cycling by intensive primary production during the austral spring-summer (Arrigo et al., 2008; Arrigo et al., 2012). "Polynyas" are seasonal sea-ice opening regions (less than 10 % of sea-ice concentration) which mainly occur from October through March along the Antarctic (Arrigo and van Dijken., 2003; Arrigo et al., 2012). Due to the

lack of ice, the open water facilitates good condition for plankton bloom such as light penetration (Yager et al, 2012). Meanwhile, "sea-ice zone (SIZ)" is a region covered with prolonged sea-ice but the concentration decreases in summer with high seasonal and inter-annual variation (Kim et al., 2015; Ducklow et al., 2015).

The Amundsen Sea is located in the western Antarctic, and hosts two coastal polynyas (the Amundsen Sea Polynya and the Pine Island Polynya) which are one of the most productive polynyas around Antarctica (Arrigo and van Dijken., 2003; Arrigo et al., 2012). Annual net primary production is ~80 and ~61 gC/m^2year in the Amundsen Sea Polynya and the Pine Island Polynya, respectively (Arrigo et al., 2012). Based on satellite observation, chlorophyll concentration in the Amundsen Sea exceeds 5 mg/m^3 in the center of both polynyas which is 2 to 3 folds higher than the other polynyas during the peak of bloom period (Arrigo et al., 2012). In addition, annual primary production in the Amundsen Sea reaches up to 2.6 gC/m^2day during the bloom period, much higher compared to the other polynyas and the Southern Ocean (Yager et al., 2012).

The Amundsen Sea is experiencing a remarkable rate of glacial melting and declining in sea-ice cover (Pritchard et al., 2012; Stammerjohn et al., 2012). Pritchard et al (2012) reported that the rate of ice sheet

thinning and grounded ice sheet loss is the highest in the Amundsen Sea. The main heat source has been addressed to be the Circumpolar Deep Water (CDW), circulating the Antarctic (Jacobs et al., 1996; Walker et al., 2007; Jacobs et al., 2012). This relatively warm, saline and dense CDW intrudes onto the Antarctic Shelves as a modified CDW (mCDW) after mixing with the surface water. In the Amundsen Sea, there are two main glacier-carved troughs extending seaward from the ice shelf fronts, the Pine Island trough and the Dotson trough. Intruded mCDW enters the cavity under the ice shelf and accelerates the basal melting (Jenkins et al., 2010; Jacobs et al., 2011; Jacobs et al., 2012). Glacial melt water (GMW) mixes with mCDW making the water mass buoyant due to the fresh water input. mCDW flows outward as "melt-laden" form in the upper water with intensive fraction of GMW mixture (Fig. 1; Wåhlin et al., 2012). Glacial melt water supplies bio-available iron and micronutrients to the polynya and affects the primary production (Yager et al., 2012).

1.4 Objectives

In the Amundsen Sea, climate-driven variability will significantly influence the carbon cycling via change in open water area and its duration, intensified surface stratification by increasing sea-ice melting, modified

primary production and remineralization influenced by glacial meltwater, efficiency of carbon export as well as sedimentation process. Several studies have focused on physical properties and water mass circulation (Wåhlin et al., 2010; Ha et al 2014), and biological processes in the Amundsen Sea (Arrigo et al., 2012; Hahm et al., 2014; Hyun et al., 2015; Kim et al., 2015). Recently, primary productivity and the efficiency of organic carbon export have been studied in localized regions, in the SIZ and inside the polynya of the Amundsen Sea (Kim et al., 2015; Ducklow et al., 2015). However, the inorganic carbon cycling is yet poorly understood. Still no full-depth, distribution of DIC concentration and its carbon isotopic values has been reported in the Amundsen Sea.

In this study, I present the first full-depth, distribution of dissolved inorganic radiocarbon in three different oceanographic regions (i.e. in the SIZ, inside the polynya and near the Dotson Ice Shelf) in the Amundsen Sea (Fig. 1). The main objectives of this study are:

- to identify the processes that control the DIC and its radiocarbon content
- to address the inorganic carbon cycling in the Amundsen Sea and its impact in the future

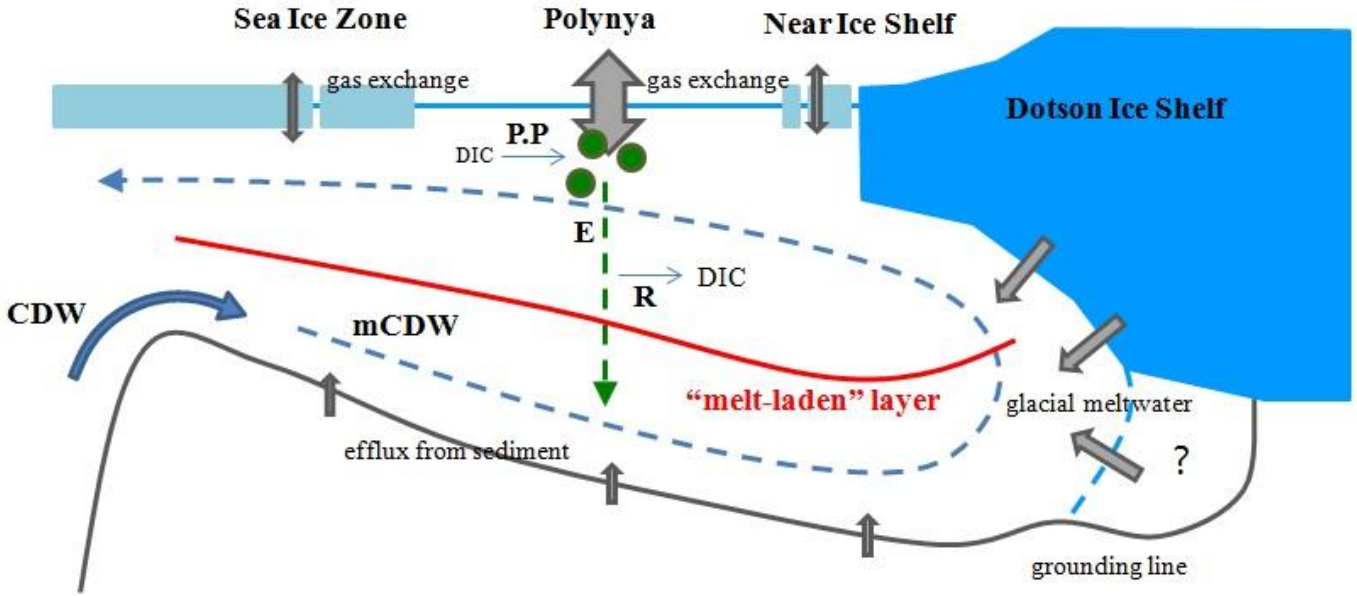

Fig. 1. Conceptual cartoon for describing the oceanographic settings and biogeochemical processes in the Amundsen Sea. Gray colored arrows indicate the major processes that may control the DIC and its radiocarbon contents. Initials stand for: CDW (Circumpolar Deep Water), mCDW (modified CDW), P.P (Primary Production), E (Export Production), R (Respiration). Green circles indicate organic carbon. Red line indicates the "melt-laden" layer (Wåhlin et al., 2010).

2. METHODS

2.1 Sample Collection and Analysis

Seawater samples for dissolved inorganic radiocarbon were collected during the cruise aboard the IBRV *Araon* from January to March in 2012 (Fig. 2). Samples were collected at three stations along the Dotson trough in the Amundsen Sea: in the sea-ice zone (SIZ) (St. 6; 72.39 °S, 117.72 °W), inside the polynya (St. 10; 73.25 °S, 114.99 °W) and near the Dotson Ice Shelf (St. 19; 74.20 °S, 112.51 °W). Bottom depths of the three sampling stations are 520 m (St. 6), 825 m (St. 10) and 1065 m (St. 19), deepening toward the Dotson Ice Shelf. Sea ice concentrations were 0 % at St. 10 and 19, and ~97 % at St. 6 during the sampling (Kim et al., 2015). Sampling period is considered as 'declining bloom period' in which average chlorophyll-a concentration and average daily productivity in the polynya significantly decreased compared to those during the peak bloom period (Lee et al., 2012; Kim et al., 2014).

From the CTD-Rosette sampler, duplicate samples from each depth were collected for DIC concentration measurement and carbon isotopes analysis. All of the sampling procedures for radiocarbon measurement in DIC followed the published guideline (Dickson et al., 2007). Briefly,

seawater from each Niskin bottle was collected into 500 ml Pyrex glass bottle (Duran) which was acid-washed and pre-combusted at 450 ℃ for 4 hours to remove organic matters. To prevent any bubbles being trapped, every sample was filled from the bottom of the sampling bottle by a silicon tube and overflowed by half of the bottle's volume. After sampling, 100 μl of saturated $HgCl_2$ solution was injected to prevent any biological processes of organic matter. The bottles were capped with greased stoppers, bound by rubber bands, and stored at room temperature until further analysis.

In the laboratory, CO_2 gas was extracted after acidification with ~4.5 ml of concentrated phosphoric acid on a vacuum line for further carbon isotopes analysis. The sketch of vacuum line is illustrated in Fig. 3. DIC extraction procedure was similar to the method described in McNichol et al (1994). Recovery of inorganic carbon by this method is ~96 % based on local surface water analysis (n=27) as a standard which was sampled from the eastern coast of South Korea.

Carbon isotopes ($\delta^{13}C$ and $\Delta^{14}C$) were analyzed at the National Ocean Sciences Accelearator Mass Spectrometry Facility at Woods Hole Oceanography Institution (NOSAMS WHOI). Radiocarbon values are reported as $\Delta^{14}C$ in per mil (‰). The result of duplicated sample analysis

(n=2) showed that uncertainties in our laboratory were less than 5 ‰ for $\Delta^{14}C$ and 0.4 ‰ for $\delta^{13}C$.

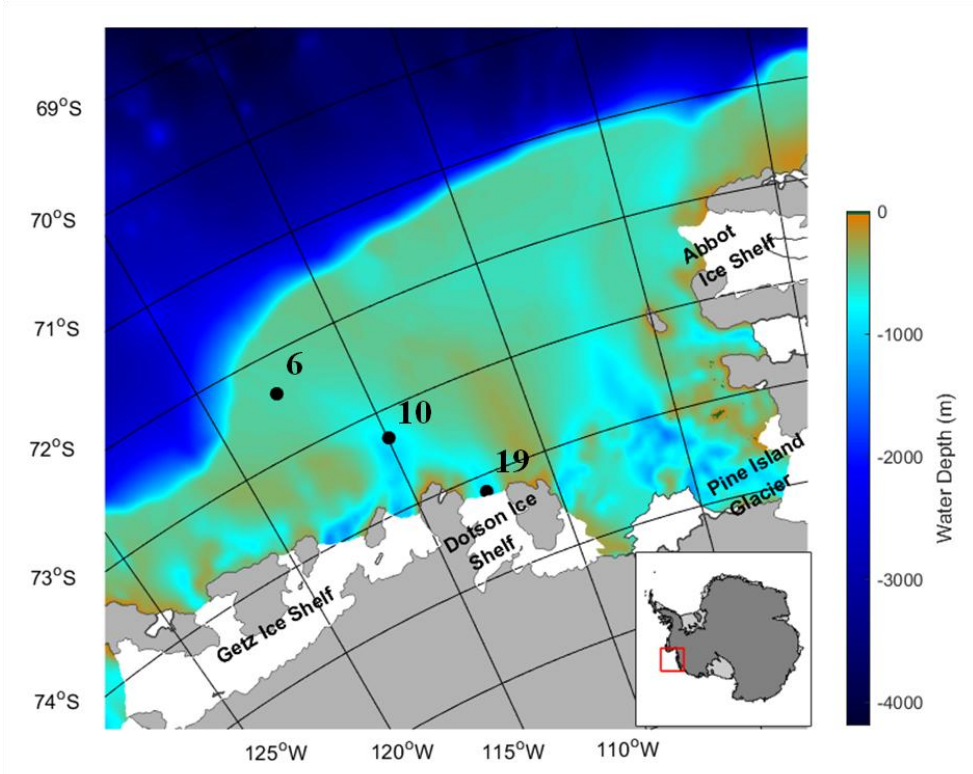

Fig. 2. Bathymetry of the Amundsen Sea and sampling locations. Sampling locations are indicated in black circles during the ANA02C cruise from Jan-Mar 2012: St.6 (in the sea-ice zone), St. 10 (inside the polynya) and St. 19 (near the Dotson Ice Shelf). Sea ice concentrations were 0 % at St. 10 and 19, and ~97 % at St. 6 during the sampling (Kim et al., 2015). Inset box indicates the location of Amundsen Sea (red square) in the Western Antarctic.

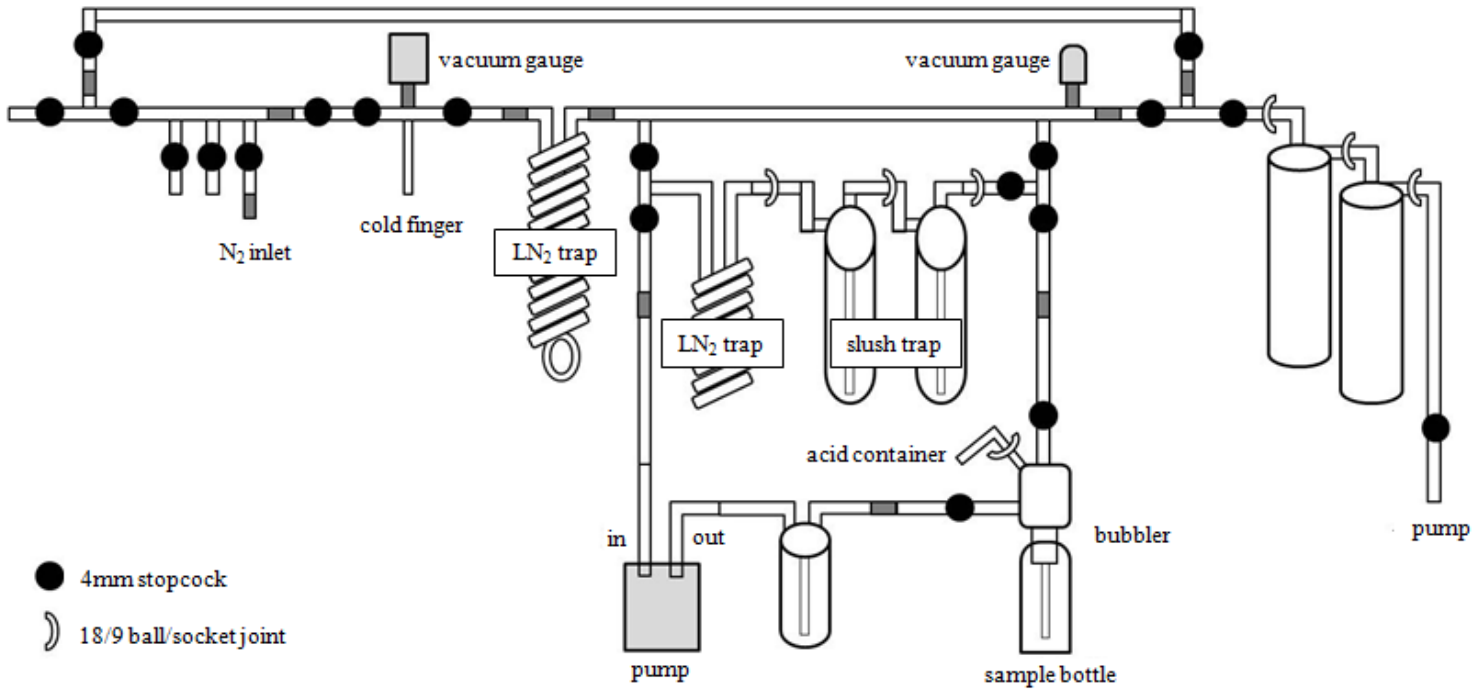

Fig. 3. Sketch of DIC extraction vacuum line.

3. RESULTS

3.1 Water Mass Structure in the Amundsen Sea

During the declining bloom period (mid-February to early March) in the Amundsen Sea, the water column can be divided into three major water masses based on the potential temperature-salinity diagram (θ-S diagram; Fig. 4): Antarctic Surface Water (AASW); Winter Water (WW) and modified CDW (mCDW) (Jacobs et al., 2012; Yager et al., 2012). WW and mCDW are the main water masses that exist during the austral winter when sea-ice is compacted over the surface layer. mCDW originates from the mixture of CDW offshore at 500-1500 m depth and WW near the shelf break, and intrudes into the shelf through glacier-carved troughs. In the Amundsen Sea, mCDW has the highest temperature and salinity, being the primary heat source for basal melting (Walker et al., 2007; Jenkins et al., 2010; Jacobs et al., 2012). Meanwhile, WW is near freezing and less saline water mass that overlies the mCDW, formed by the sea ice production during the previous winter (Yager et al., 2012). In austral spring when the sea-ice starts to melt and the polynya opens, freshened and warmed surface water of WW becomes AASW. AASW was observed in a scattered distribution on the T-S diagram and different temperature and salinity range

reflects the degree of surface warming and residual sea-ice melting (Tortell et al., 2012). In late austral summer when the open water region starts to shrink, AASW cools to the freezing point and becomes saline due to the brine rejection during sea-ice production. Eventually, seasonally freshened and warm AASW returns to WW closing a one-year cycle.

In the deep layer (σ_t > 27.6), high temperature (~0.5 ℃) and high salinity (~34.5 psu) of mCDW was observed at all three stations (Fig 4). The temperature and salinity property of mCDW detected in this study, however, was relatively lower compared to mCDW signature in the previous year in the Amundsen Sea (θ~1 ℃, S~34.6, Yager et al., 2012). This implies that intrusion of mCDW in 2012 was weak and/or it was more modified by the mixture of cooler and fresher WW. Especially, mCDW in the SIZ showed relatively lower temperature and salinity values compared to the other two stations, implying a more modification.

The coldest and saline WW was observed in the intermediate layer (27.4 < σ_t < 27.5) above the mCDW (Fig. 4). In the SIZ and inside the polynya, WW showed a similar temperature and salinity property (θ~ −1.7 ℃, S~34.1 psu). Potential temperatures were near the freezing point of seawater (~ −2 ℃; red straight line in Fig. 4). In contrast, WW near the ice shelf was observed to be slightly warmer.

AASW was observed in a wider range in the upper layer (σ_t < 27.2; Fig. 4). The highest temperature (~ −1.1 ℃) and the lowest salinity (~33.5 psu) were observed in the surface of polynya due to the extended solar radiation and input of sea-ice melt. Considering the sampling period (late bloom), surface temperatures inside the polynya in this study were cooler compared to the temperatures during the peak bloom (−1 to 0 ℃; Yager et al., 2012; Miles et al., 2014). Temperatures in the SIZ and near ice shelf ranged between −1.5 ℃ and the freezing point of seawater (~ −2 ℃), more similar to WW. Salinity of the surface water near the ice shelf (~33.8 psu) was slightly higher compared to that in the SIZ (~33.6 psu).

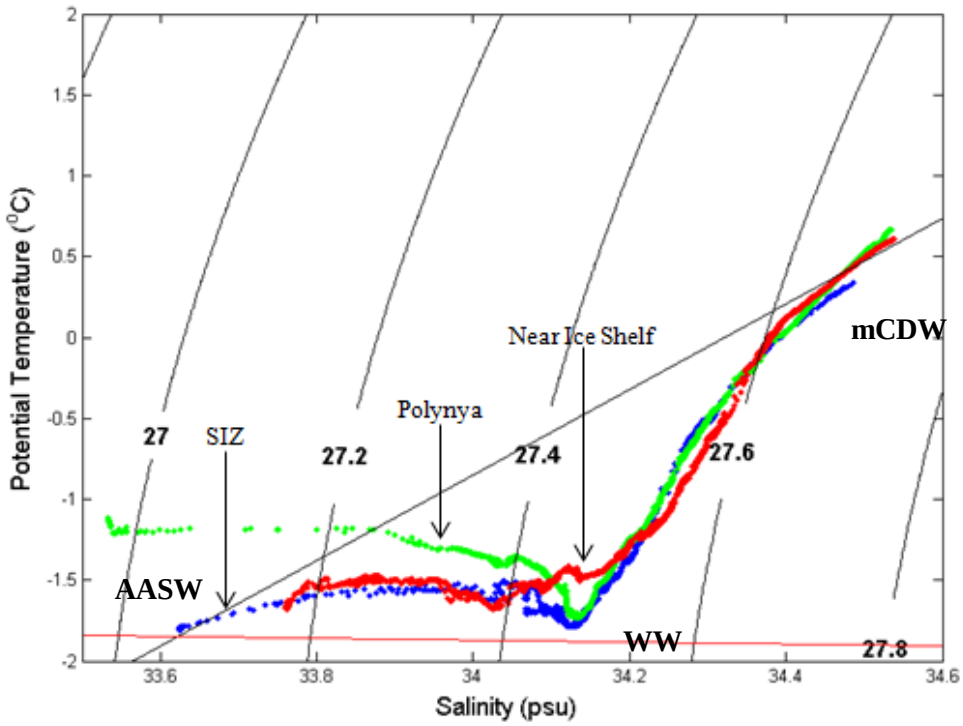

Fig. 4. θ-S diagram of the sampling stations in the Amundsen Sea: in the SIZ (St. 6; blue), inside the polynya (St. 10; green) and near the Dotson Ice Shelf (St. 19; red).The initials denotes the water mass of Antarctic Surface Water (AASW), Winter Water (WW) and modified- Circumpolar Deep Water (mCDW). Labeled black contours indicate σ_t as density. Black straight line is the mixing line between glacial meltwater (GMW) and mCDW, similar to the "Gade Line" (Gade, 1979; Wåhlin et al., 2010). Red straight line represents the freezing point of seawater. Units of potential temperature and salinity are ℃ and psu, respectively.

3.2 Carbon Isotopes Ratios ($\delta^{13}C$ and $\Delta^{14}C$)

Sea Ice Zone

In the SIZ, $\Delta^{14}C$ values of DIC ranged narrowly between −154 ‰ and −147 ‰ (Table 1, Fig. 5). $\Delta^{14}C$ value in the surface was significantly lower (−153 ‰) compared to those in the polynya and near the ice shelf. $\Delta^{14}C$ value slightly increased to −148 ‰ at 100 m depth and remained similar (−147 ±1 ‰; n=3) from 100 to 400 m depth. The radiocarbon value near the bottom was depleted (−154 ‰) compare to the upper layer.

$\delta^{13}C$ values of DIC were in the range of −0.2 to 0.8 ‰ (Table 1, Fig. 6). $\delta^{13}C$ value was the highest (0.8 ‰) in the surface. Below 100 m depth, $\delta^{13}C$ values were lower compared to the surface value, average of nearly 0 ‰ (0.0 ±0.3 ‰; n=4).

Inside the Polynya

$\Delta^{14}C$ values inside the polynya ranged from −157 to −129 ‰ (Table 1, Fig. 5). The surface $\Delta^{14}C$ value was the highest (−136 ±1 ‰; n=2) compared to the other surface values. This was similar to the average surface $\Delta^{14}C$ value of suspended POC measured inside the polynya (−136 ±7 ‰; n=3, Kim et al., 2015). Although $\Delta^{14}C$ value decreased to −144 ‰ at 70 m depth, enriched radiocarbon signals of −129 ‰ and −134 ‰ were observed at 130

m and 250 m depth, respectively. These two values are significantly higher compared to the other values at similar depths in the SIZ and near the ice shelf. Also, the highest value (−129 ‰) among the three stations was observed inside the polynya at a depth of 130 m. $\Delta^{14}C$ value deceased to −147 ‰ at 320 m depth, similar to the $\Delta^{14}C$ value between 100 m and 400 m at the other two stations. In deep layer (> 500 m), $\Delta^{14}C$ value gradually decreased with depth, and was most depleted (−159 ±3 ‰; n=2) near the bottom.

$\delta^{13}C$ values of DIC ranged between −0.1 and 2.1 ‰ (Table 1, Fig. 6). In the surface, $\delta^{13}C$ value was the highest (2.1 ±0.1 ‰; n=2) inside the polynya as well as among the three stations. $\delta^{13}C$ value decreased to 0.3 ‰ at 70 m depth, and remained nearly constant (0.2 ± 0.1 ‰; n=5) until 540 m depth. $\delta^{13}C$ value was slightly lower near the bottom (−0.1 ±0.3 ‰; n=2).

Near the Dotson Ice Shelf

$\Delta^{14}C$ values near the Dotson Ice Shelf generally decreased from surface to bottom, ranging between −140 to −162 ‰ (Table 1, Fig. 5). The surface $\Delta^{14}C$ value of DIC was high up to −140 ‰, which was slightly lower than that in the surface water inside the polynya (−136 ‰). This was similar to the surface $\Delta^{14}C$ value of suspended POC measured in the same station

(−144 ‰; Kim et al., 2015). $\Delta^{14}C$ value remained uniform (−146 ±2 ‰; n=4) between 100 m and 410 m, similar to $\Delta^{14}C$ values in 100−400 m layer in the SIZ (average of −147 ‰) and at 410 m depth in the polynya (−147 ‰). In the deep layer (> 600 m), $\Delta^{14}C$ values decreased with increasing depth, and was the lowest (−161 ±1 ‰; n=2) near the bottom.

$\delta^{13}C$ values of DIC near the ice shelf ranged between 0.2 to 1.0 ‰ (Table 1, Fig. 6). $\delta^{13}C$ value was the highest at the surface (1.0 ‰) then decrease to 0.3 ‰ at 100 m depth. Slightly higher $\delta^{13}C$ value was observed at a depth of 190 m (0.6 ‰). $\delta^{13}C$ values remained nearly constant (0.3 ±0.1 ‰; n=5) below 200 m. $\delta^{13}C$ value at near the bottom was slightly lower (0.2 ‰), implying that the bottom process is important.

$\delta^{13}C$ value of −0.6 ‰ at 410 m (Table 1, Fig. 6 in parentheses) was regarded erroneous because it was found that only about ~30 % of expected volume existed in the sample tube when cracked at NOSAMS for isotopic measurement. However, $\Delta^{14}C$ value was proved to be the same as the value independently obtained (−146 ‰). This is believed to be that the delta notation, $\Delta^{14}C$ value, is not affected by isotopic fractionation (Stuiver and Polach, 1977).

Table 1. $\Delta^{14}C$ and $\delta^{13}C$ values for samples collected at three different sites in the Amundsen Sea during January-March 2012

Oceanographic Setting	Depth (m)	$\Delta^{14}C$ (‰)	$\delta^{13}C$ (‰)
Sea Ice Zone	3	-153	0.8
(St. 6)	100	-148	-0.2
	190	-147	0.3
	410	-147	-0.2
	515	-154	0.2
Inside Polynya	2	-136	2.1
(St. 10)	20	-135	2.0
	70	-144	0.3
	130	-129	0.2
	250	-134	0.2
	320	-147	0.1
	540	-153	0.2
	810	-157	0.1
	810 (duplicate)	-161	-0.3
Near Ice Shelf	10	-140	1.0
(St. 19)	100	-147	0.3
	190	-144	0.6
	220	-147	0.4
	410*	-146	-0.6*
	410 (duplicate)	-146	0.3
	700	-157	0.4
	1020	-160	0.3
	1064	-162	0.2

* Regarded as outlier (see text)

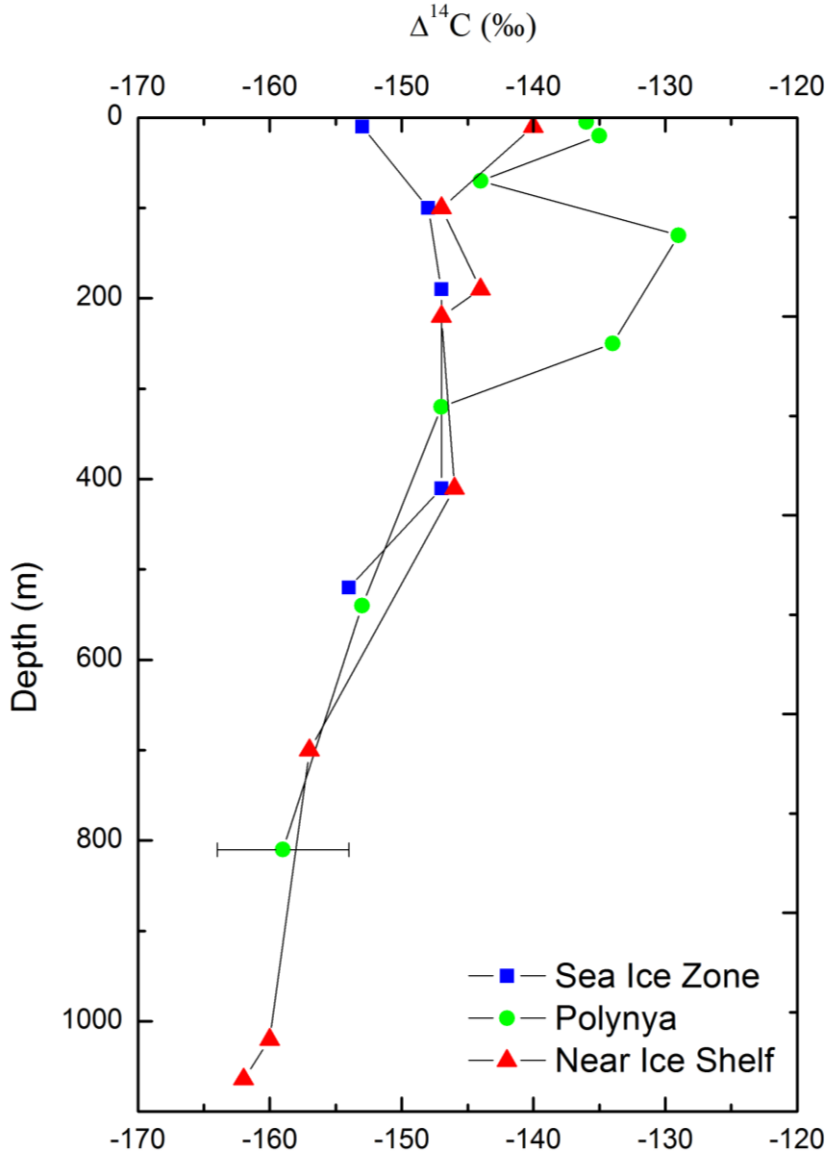

Fig 5. Distribution of $\Delta^{14}C$ values versus depth (m) in the Amundsen Sea: in the SIZ (St. 6; blue square), inside the polynya (St. 10; green circle) and near the Dotson Ice Shelf (St. 19; red triangle). The unit of $\Delta^{14}C$ value is reported in per mil (‰).

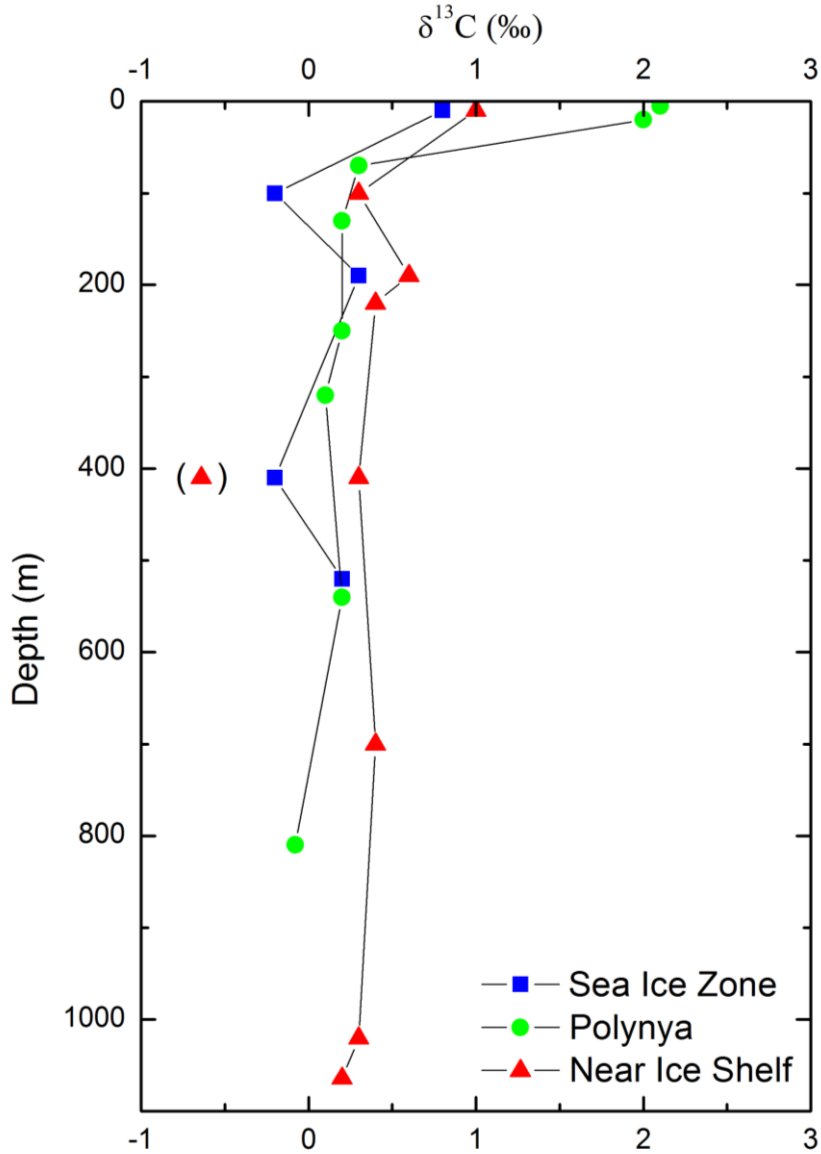

Fig. 6. Distribution of $\delta^{13}C$ values versus depth (m) in the Amundsen Sea: in the SIZ (St. 6; blue square), inside the polynya (St. 10; green circle) and near the Dotson Ice Shelf (St. 19; red triangle). The unit of $\delta^{13}C$ value is reported in per mil (‰). Measurement inside parenthesis (at 410 m depth; near ice shelf) indicates the outlier (see text).

4. DISCUSSION

4.1 Distribution of Dissolved Inorganic Radiocarbon in the Amundsen Sea

A plot of $\Delta^{14}C$ values versus density (σ_t) instead of depth (Fig. 7) may better visualize the relationship between the water mass structure and the distribution of $\Delta^{14}C$ values. In the Amundsen Sea, average $\Delta^{14}C$ value of the surface layer was −141 ‰ (Fig. 7). This value was much lower than mean surface value in Weddell Sea (−92 ‰) which Weiss et al (1979) reported as the lowest $\Delta^{14}C$ value observed. Especially, the $\Delta^{14}C$ value in the surface water in the SIZ was considered to be lower compared to other surface radiocarbon measurements conducted previously around the Antarctica (Weiss et al., 1979; Leboucher et al, 1999; Key and McNichol, 2012). Oceanography setting of limited gas exchange with the atmosphere (sea-ice coverage) and depleted radiocarbon source (intrusion of CDW) is likely the reason for this lowest observed $\Delta^{14}C$ value of SIZ (−153 ‰) in the Amundsen Sea.

In the surface layer (σ_t < 27.2), radiocarbon distribution showed a distinctive spatial variation (−141 ±8 ‰; n=4) associated with sea-ice

coverage (Fig. 7). In the SIZ where sea-ice concentration is high, surface $\Delta^{14}C$ value was significantly lower (−153 ‰) compared to the open water regions (i.e. inside the polynya and near ice shelf). Surface $\Delta^{14}C$ values in open water regions were higher by ~20 ‰. The main source of radiocarbon in the ocean is the atmospheric radiocarbon which transfers into the surface ocean by air-sea CO_2 exchange. This implies that the coverage of sea-ice is an important factor controlling the radiocarbon distribution in the surface waters by limiting the air-sea gas exchange.

Below the surface layer to ~400 m depth ($27.2 < \sigma_t < 27.55$), $\Delta^{14}C$ values are nearly constant (−147 ±1 ‰; n=9), except for the layer between 100 m and 300 m depth inside the polynya (Fig. 5, Fig. 7). WW is the major water mass in this intermediate layer (100−400 m depth). Especially, I choose $\Delta^{14}C$ value of −147 ‰ as an end-member of WW where the lowest potential temperature (~ −1.8 ℃) and high salinity (~34.1 psu) were observed (190 m depth in the SIZ, 320 m depth inside the polynya). In contrast, significantly enriched radiocarbon signatures were interestingly observed inside the polynya at 100−300 m depth (−132 ±4 ‰; n=2). Compared to SIZ and near ice shelf, polynya has the potential source of 'young' or enriched radiocarbon from remineralization of sinking particles produced by high primary production in the polynya surface and massive

CO_2 uptake by air-sea gas exchange. This aspect is discussed in more details in section *4.2.4 Remineralization of Sinking Particles* and section *4.3 Air-Sea Gas Exchange of CO_2*.

In the deep layer (σ_t > 27.55), $\Delta^{14}C$ values of mCDW were much lower (−158 ±3 ‰; n=6) than the upper layer (Fig. 7). These values was comparable to $\Delta^{14}C$ value of CDW (−160 ‰; Key and McNichol, 2012), confirming that CDW was the major source. The $\Delta^{14}C$ value decreased with depth along the mixing line between CDW and WW. $\Delta^{14}C$ value near the bottom of SIZ was nearly 5 ‰ higher compared to the other two stations. This observation also supports that mCDW in the SIZ was more modified (relatively colder and fresher) as shown in the θ-S diagram (Fig. 4).

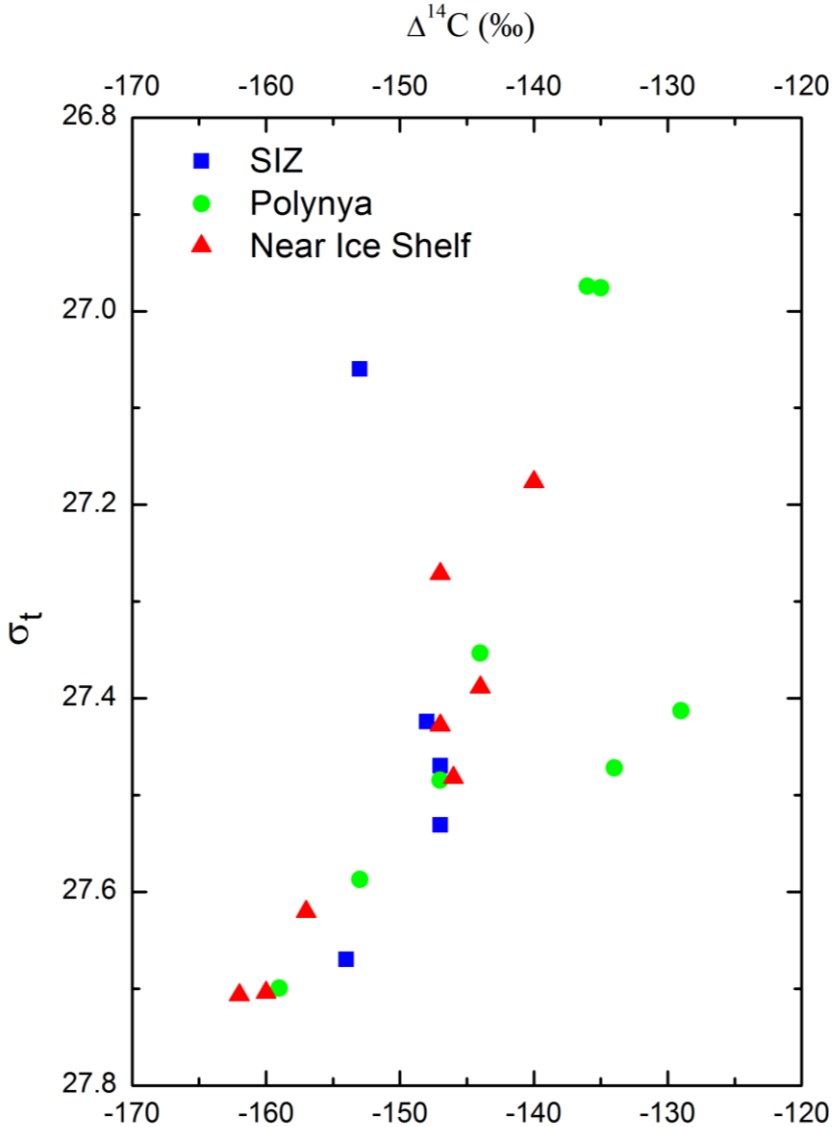

Fig. 7. Distribution of $\Delta^{14}C$ values versus σ_t in the Amundsen Sea: in the SIZ (St. 6; blue square), inside the polynya (St. 10; green circle) and near the Dotson Ice Shelf (St. 19; red triangle). The unit of $\Delta^{14}C$ value is reported in per mil (‰).

4.2 Potential Sources of Carbon to DIC in the Amundsen Sea

4.2.1 Primary Productivity in the Surface Layer

In the surface water, DIC concentration and stable isotopic composition ($\delta^{13}C$) of DIC together can provide information on spatial variation in primary productivity in the Amundsen Sea. Marine phytoplankton fractionates stable carbon isotope by nearly −20 ‰ in non-polar region, and −30 ‰ in the Antarctic (Rau et al., 1989; Fischer, 1991) during the photosynthesis. Therefore, primary production makes the surface ocean depleted in DIC concentration and nutrients, and enriched in $\delta^{13}C$ value.

As a proxy for primary productivity at different stations, I used the reported carbon uptake rates of phytoplankton in the surface which was measured during the same cruise (Kim et al., 2015). The column integrated (i.e. euphotic zone depth) uptake rate was the highest in the polynya (~343 mg C/m^2day), and slightly higher near the ice shelf (~195 mg C/m^2day) than the SIZ (~161 mg C/m^2day). Higher carbon uptake rate indicates higher primary productivity which decreases DIC concentration and cause higher isotopic fractionation.

The lowest DIC concentration (T. S. Rhee; unpublished results) and the highest $\delta^{13}C$ value (2.1 ‰) were observed in the surface water inside the polynya where the primary production was the highest (Fig. 6). According

to nutrient vertical profile from surface to 100 m depth in the same study area and sampling period (Kim et al., 2015), phosphate concentration showed the highest drawdown of ~1.4 μM in the surface water of the polynya compared to ~0.7 μM in the SIZ and ~0.5 μM near the ice shelf. Based on a simple Redfield ratio (C:N:P=106:16:1), phosphate depletion corresponds to a carbon uptake of ~148 μmol/kg (= 1.4 μM × 106) in the polynya. Assuming that the surface water originates from WW with DIC concentration of 2215 μmol/kg at 100 m depth (Mu et al., 2014), surface DIC concentration in the polynya is estimated to have decreased to 2067 μmol/kg. This estimate was comparable to the measured DIC concentration inside the polynya (T. S. Rhee; unpublished results).

Compared to the polynya, surface $\delta^{13}C$ values in the SIZ and near ice shelf were similar (Fig. 6) but surface pCO_2 was supersaturated near the Dotson Ice Shelf (Yager et al., 2012; Mu et al., 2014; Hahm et al., 2014). Based on the same calculation above, phosphate depletion corresponds to a carbon uptake of ~74 μmol/kg in the SIZ and ~53 μmol/kg near the ice shelf. However, supersaturated pCO_2 measurements indicate DIC addition from the deep layer to the surface where upwelling is prominent in front of the Dotson Ice Shelf (Yager et al., 2012; Mu et al., 2014; Hahm et al., 2015).

4.2.2 Glacial Meltwater

To determine the influence of GMW input to both DIC concentration and $\Delta^{14}C$, CO_2 concentration of pure GMW was first estimated. I used average gas amount of 0.11 cm^3 STP/kg and average CO_2 abundance of 0.0270 % of the Byrd ice core from 1068 to 1469 m depth (Fireman and Norris, 1982). The calculated CO_2 content was 2.97×10^{-8} cm^3 STP/kg, which was equivalent to 1.3 μmol/kg of C. For radiocarbon content in GMW, I assumed $\Delta^{14}C$ value to be radiocarbon dead (i.e. −1000 ‰) because $^{14}CO_2$ trapped in ice core below 1068 m depth had been isolated from the atmosphere for sufficiently long time compared to the half-life of radiocarbon. According to Fireman and Norris (1982), ^{14}C age of Byrd ice core from 1071 m depth was greater than 8000 years.

To estimate the change in both DIC concentration and $\Delta^{14}C$ value by GMW input, the following mass balance calculation was used for two end-members mixing. Two cases were considered: between (1) WW and GMW; (2) CDW and GMW.

$$F_{WW/CDW} + F_{GMW} = 1$$

$$[DIC]_{WW/CDW}F_{WW/CDW} + [DIC]_{GMW}F_{GMW} = [DIC]_{mix}$$

$$\Delta^{14}C_{WW/CDW}[DIC]_{WW/CDW}F_{WW/CDW} + \Delta^{14}C_{GMW}[DIC]_{GMW}F_{GMW} = \Delta^{14}C_{mix}[DIC]_{mix}$$

where F is fraction, [DIC] is DIC concentration, and $\Delta^{14}C$ is radiocarbon value of WW or CDW (WW/CDW), glacial meltwater (GMW) and mixture of two end-members (mix). I used $[DIC]_{WW}$ = 2215 μmol/kg (Mu et al., 2014), $\Delta^{14}C_{WW}$ = −147 ‰ (in this study) for WW, and $[DIC]_{CDW}$ = 2270 μmol/kg (Hoppema et al., 2000), $\Delta^{14}C_{CDW}$ = −160 ‰ (Leboucher et al., 1999; Key and McNichol, 2012) for CDW. For GMW, $[DIC]_{GMW}$ = 1.3 μmol/kg, $\Delta^{14}C_{GMW}$ = −1000 ‰ were used. Fractions of GMW (F_{GMW}) were previously estimated to be 0.3 to 0.8 % along the Dotson trough based on excess He (Kim et al., 2016).

The input of glacial meltwater (GMW) mainly controlled DIC concentration rather than radiocarbon signature (Fig. 8). According to the mass balance calculation above, GMW fraction up to 1 % depleted both DIC concentrations of WW and CDW as by up to ~22 μmol/kg. However, because of negligible amount of carbon containing inside GMW, $\Delta^{14}C$ values of WW and CDW did not changed after mixing with GMW. Especially, in the polynya, DIC concentration greatly deceased at 320 m depth (σ_t ~27.5; T. S. Rhee; unpublished results) compared to the other two stations. This isopycnal layer was consistent to "melt-laden" layer where maximum peak of GMW fraction was observed (Wåhlin et al., 2010; Kim et al., 2016).

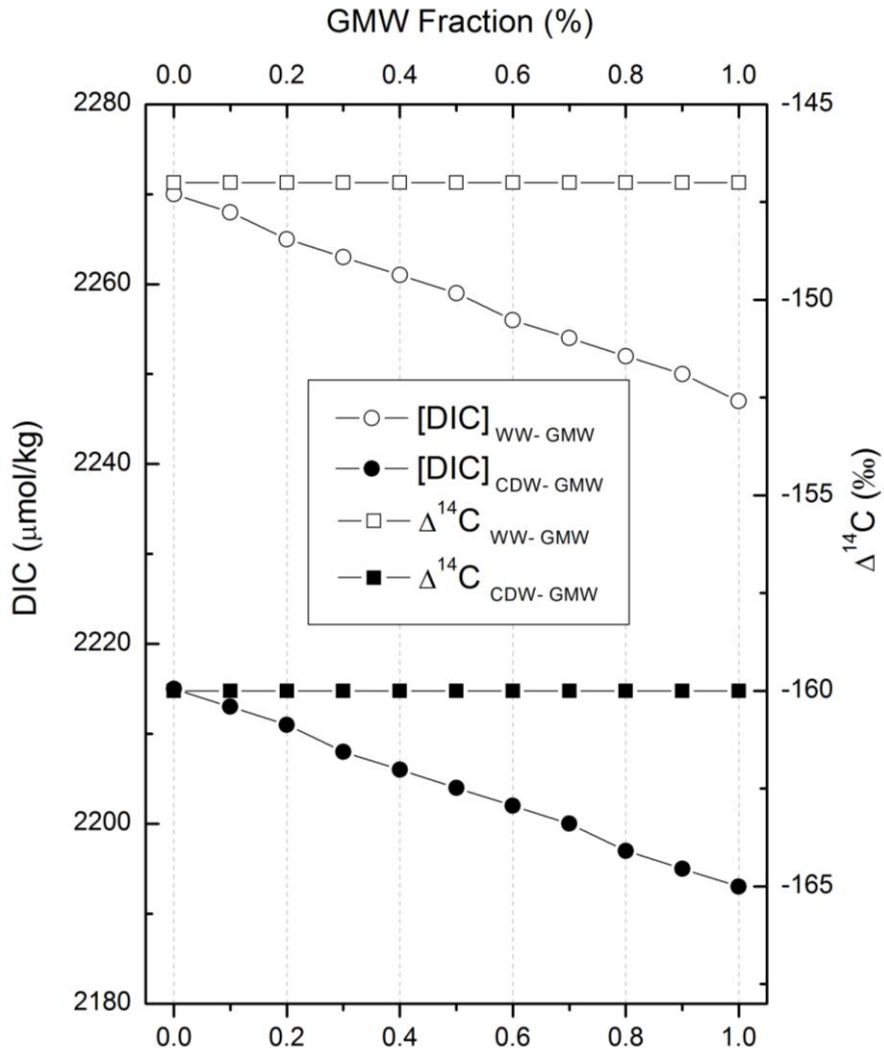

Fig. 8. Change in DIC concentration and $\Delta^{14}C$ value between two end-member mixing (WW-GMW and CDW-GMW) versus GMW fraction (%). Open circle and square indicate DIC concentration and $\Delta^{14}C$ value between WW-GMW mixing, respectively. Filled circle and square indicate DIC concentration and $\Delta^{14}C$ value between CDW-GMW mixing, respectively.

4.2.3 Benthic Efflux

To examine the influence of benthic efflux to DIC budget, I estimated the carbon flux from the sediment in the Amundsen Sea. According to Kim et al (2016), benthic nutrient fluxes in the polynya (0.13 mmol N/m^2d, 0.017 mmol P/m^2d) were much higher than those measured in SIZ (0.09 mmol N/m^2d, 0.004 mmol P/m^2d) and near the ice shelf (0.09 mmol N/m^2d, 0.005 mmol P/m^2d), respectively. Using the measured C:N:P ratio of sediment−seawater exchange flux in Kim et al (2016), average benthic effluxes of carbon from sediment were estimated to be ~0.8 mol C/m^2yr in the polynya compared to those in the SIZ (~0.3 mol C/m^2yr) and near the ice shelf (~0.5 mol C/m^2yr). Assuming DIC concentration of 2255 μmol/kg (mCDW; Mu et al., 2014) and average seawater density of 1030 kg/m^3, DIC inventory of mCDW in average 300 m water column above bottom was ~700 mol/m^2 (= 2255 μmol/kg × 1030 kg/m^3 × 300 m). This exercise points out that the contribution of annual average benthic effluxes in the Amundsen Sea was negligible to the DIC budget in the water column.

4.2.4 Remineralization of Sinking Particles

In this section, I estimated the radiocarbon input from remineralization of sinking particulate organic carbon (POC) derived from the surface into the deep water column in the polynya. The annual net primary production rate of the Amundsen Polynya is ~80 gC/m^2 (Arrigo et al., 2012). To be conservative, I assumed that half of the primary production (~40 gC/m^2) is exported below 100 m depth. DIC inventory below 100 m in each square meter was ~1600 mol/m^2 (= 2215 μmol/kg × 1030 kg/m^3 × 700 m), assuming DIC concentration of 2215 μmol/kg at depth of ~100 m (Mu et al., 2012). This inventory is equivalent to 19000 gC/m^2. Remineralization of sinking POC contributed less than 1 % of deep DIC inventory, implying negligible change of radiocarbon signature in the deep layer.

A massive decrease of POC flux between 60 m and 150 m depth (~24 $mmol/m^2day$) has been reported, suggesting bacterial respiration remineralized most of the organic carbon exported from the surface (Ducklow et al., 2015). Assuming all POC has been remineralized into DIC during the average bloom period of the Amundsen Sea polynya (~70 days; Arrigo et al., 2012), bacterial respiration (based on annual, ~2 mol/m^2) also contributed nearly 1 % of DIC inventory within 60−150 m layer (~200 mol/m^2 = 2215 μmol/kg × 1030 kg/m^3 × 90 m). In addition, input of

organic carbon remineralized with surface radiocarbon signature (−136 ‰) would only increase $\Delta^{14}C$ value by less than 1 ‰ based on mass balance calculation.

4.3 Air-Sea Gas Exchange of CO_2

Since the input from the sources discussed in the previous section is negligible, air-sea gas exchange is likely to be the primary process to increase radiocarbon signature in the upper layer (Fig. 5, 7). From surface to ~300 m depth, inside the polynya, $\Delta^{14}C$ values (average of −136 ±5 ‰; n=5) are higher by up to ~20 ‰ than the other two stations. If the radiocarbon distribution before air-sea exchange is determined, the difference between the measured $\Delta^{14}C$ values and the initial radiocarbon distribution integrated over the water column is equivalent to the amount of atmospheric radiocarbon input via gas exchange (similar to estimation of bomb-^{14}C inventory). Unfortunately, no radiocarbon measurements during the austral winter or at the beginning of polynya opening are available in the Amundsen Sea polynyas. Most of the measurements were conducted outside the Antarctic shelves and/or during the austral spring-summer period (Weiss et al, 1979; Leboucher et al., 1999; Key and McNichol, 2012).

To estimate the air-sea CO_2 exchange, two scenarios of temporal change in radiocarbon distribution were assumed (Fig. 9). The difference between the two scenarios was the initial distribution of radiocarbon (i.e. baseline) during the austral winter when sea-ice covered the entire Amundsen Sea and the water column had been replenished. When the

polynya opens, primary production (i.e. decreasing DIC concentration and pCO_2) facilitates absorption of atmospheric CO_2 and consequently increases the $\Delta^{14}C$ in the water column. Briefly, I calculated the polygon areas (between measured $\Delta^{14}C$ value and baseline) and converted into an equal-area rectangle. Radiocarbon penetration depth and average $\Delta^{14}C$ value in the DIC inventory are defined from the converted rectangle. Based on a simple mass balance between two end-members, the atmosphere ($\Delta^{14}C$ ~ +40 ‰; Graven et al., 2012) and the initial $\Delta^{14}C$ value, the fraction of net atmospheric input was estimated. Assuming the isotopic equilibration of radiocarbon in each box area as a simple box model, CO_2 exchange time τ (i.e. residence time) was calculated from the following equation (Weiss et al., 1979):

$$\tau = \frac{t}{\ln\left(\frac{\Delta^{14}C_{inital} - \Delta^{14}C_{atm}}{\Delta^{14}C_t - \Delta^{14}C_{atm}}\right)}$$

where $\Delta^{14}C_{inital}$ is the initial $\Delta^{14}C$ value referring to the beginning of equilibrium process, $\Delta^{14}C_{atm}$ is the mean $\Delta^{14}C$ value of atmospheric CO_2 in the southern hemisphere (~ +40 ‰; Graven et al., 2012), t is the time after the beginning of equilibrium process and $\Delta^{14}C_t$ is observed $\Delta^{14}C$ value at

time t. Considering the average polynya opening time in the Amundsen Sea (November 11; Arrigo et al., 2012), time t is approximately 3 months by the sampling period (mid-February). To estimate the air-sea CO_2 exchange rate, τ was applied to the fraction of net atmospheric input in the DIC inventory. The errors were propagated in calculations (Table 2).

Scenario 1

Scenario 1 assumes a homogenous radiocarbon distribution of −160 ‰ ($\Delta^{14}C$ value of CDW) in the initial stage (Fig. 9a). In this case, the entire water column was ventilated by CDW during the austral winter, and higher $\Delta^{14}C$ values observed in summer was caused by atmospheric CO_2 input. Converted boxes at the three stations are shown in Fig 9a. Simple mass balance between two end-members, the atmosphere and CDW, indicated ~5, ~13 and ~10 % of net atmospheric input in the SIZ, polynya and near ice shelf, respectively. In the SIZ, for example, 5 % of DIC inventory area was ~57 mol/m^2 (= 2215 μmol/kg × 1030 kg/m^3 × 500 m × 5 %) with DIC concentration of 2215 μmol/kg (Mu et al., 2012), average seawater density of 1030 kg/m^3 and penetration depth of 600 m in the box area. CO_2 exchange time τ in the SIZ was ~ 58 months. If I apply the calculated τ to DIC inventory of 5 % net atmospheric fraction, air-sea CO_2 exchange rate in

the SIZ was 32 ±32 mmol/m^2day (1 month = 30 days) (Table 2). Following the same approach, air-sea CO_2 exchange rates in the polynya and near the ice shelf were 168 ±68 mmol/m^2day and 93 ±47 mmol/m^2day, respectively (Table 2).

Calculated CO_2 exchange rates based on scenario 1 appear highly overestimated in all three regions compared to the reported values in the Amundsen Sea (Mu et al., 2014; Tortell et al., 2012). Mu et al (2014) reported that spatially averaged CO_2 flux was ~18 mmol/m^2day over the entire open water region and doubled to ~36 mmol/m^2day in the central polynya (December to early January). Tortell et al. (2012) reported that low surface pCO_2 (as low as 100 μatm) persisted until late summer in the Amundsen Sea (mid-January to mid-Februray), and air-sea CO_2 flux was significantly higher (~42 mmol/m^2day) in the ice-free polynya region. However, estimated CO_2 exchange rate based on $\Delta^{14}C$ in the center of the polynya was 4 to 5 folds higher than air-sea exchange rates based on pCO_2 measurements in the other studies. Even average CO_2 exchange rate of the two ice-free regions (130 ±84 mmol/m^2day; inside the polynya and near the ice shelf) was 3 to 7 folds higher than the previous estimates. In addition, CO_2 exchange rate in the SIZ was considerably high even though sea-ice concentration was nearly 100 % during the sampling period (Kim et al, 2015)

although Bates (2006) argued that air-sea flux of CO_2 is negligible when sea-ice concentration is near 100 %.

Scenario 2

In scenario 2, the initial radiocarbon distribution was assumed to be the same as the observed distribution in the SIZ, i.e., average $\Delta^{14}C$ value of −150 ‰ (Fig. 9b). This scenario assumes that the residence time in the upper layer above (m)CDW was longer than polynya opening period and air-sea exchange was negligible in the SIZ. Simple mass balance calculation between the atmosphere and $\Delta^{14}C_{inital}$ of −150 ‰ yielded ~8 and ~5 % of net atmospheric input in the polynya and near ice shelf, respectively. Following the same approach as scenario 1, air-sea CO_2 exchange rates corresponded to 49 ±33 mmol/m^2day and 11 ±11 mmol/m^2day in the polynya and near ice shelf, respectively (Table 2).

More realistically, considering the previously reported CO_2 exchange rates, the initial radiocarbon distribution was likely to lie between scenario 1 and scenario 2, but rather closer to scenario 2. Average CO_2 exchange rate in the open water was 30 ±36 mmol/m^2day (Table 2), slightly smaller than the reported values observed in the similar time period (Tortell et al., 2012). Initial radiocarbon distribution was likely to have been slightly

lower than $\Delta^{14}C$ value of −150 ‰. This implies that air-sea exchange was not negligible in the SIZ. Although the sea-ice concentration was ~100 % during the sampling period, seasonal and inter-annual variability of sea-ice concentration in the SIZ was observed (Kim et al., 2015). Increased primary productivity in the SIZ, during the early bloom period, could drawdown the surface pCO_2, and have driven small but significant CO_2 uptake when the sea-ice concentration was not 100 %. Applying the average open water area of the Amundsen Sea polynya (~27000 km^2; Arrigo et al., 2012) and open duration period to nearly 4 months, net CO_2 uptake in the Amundsen Sea was estimated to be ~1.2 Tg C. This simple calculation suggests that the Amundsen Sea accounts for ~3 % of CO_2 uptake by total Southern Ocean (40 Tg C; Takahashi et al., 2009), although the area accounts for only 0.08 %.

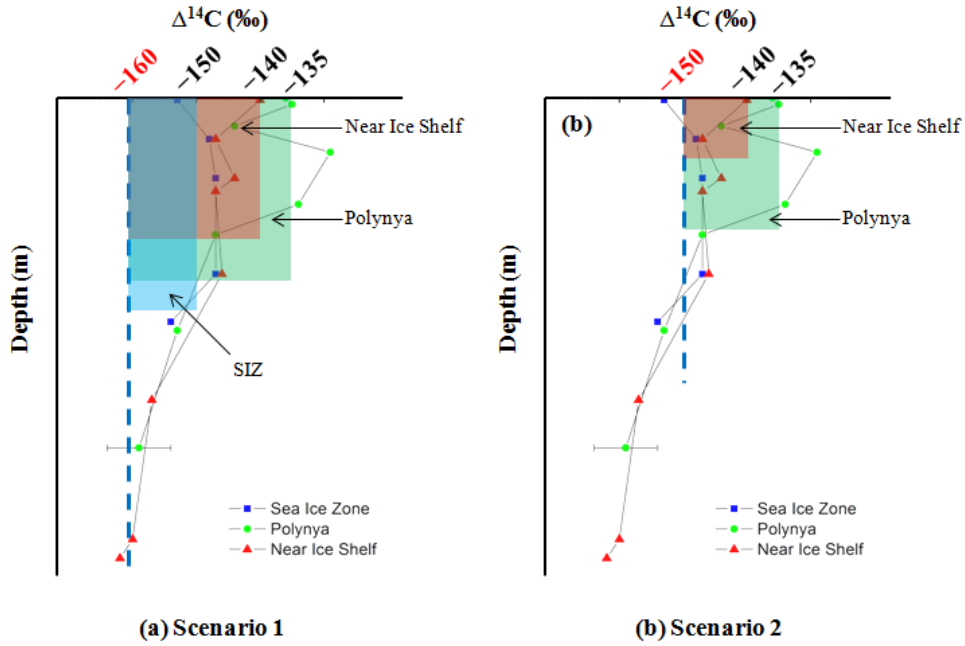

Fig. 9. Initial distribution of radiocarbon used for (a) scenario 1 and for (b) scenario 2. Calculated area of net atmospheric radiocarbon input is converted into a rectangle: blue box (in the SIZ); green box (polynya) and red box (near ice shelf). Blue dashed line and $\Delta^{14}C$ value in red color indicates the initial distribution of radiocarbon.

Table 2. Box area, fraction of atmospheric input, fraction of DIC inventory, CO_2 exchange time and calculated air-sea CO_2 exchange rate in the three stations based on scenario 1 and scenario 2.

Oceanographic Setting	Box Area		Fraction of Atmospheric Input (%)	Fraction × DIC inventory (mol/m^2)	CO_2 exchange time τ (months)	Air-Sea CO_2 Exchange Rate ($mmol/m^2day$)
	Depth (m)	$\Delta^{14}C_t$ (‰)				
Scenario 1 ($\Delta^{14}C_{initial} = -160$ ‰)						
Sea Ice Zone	500	-150	5 ±4	57 ±40	58 ±41	32 ±32
Inside Polynya	400	-135	13 ±4	113 ±32	22 ±6	168 ±68
Near Ice Shelf	350	-140	10 ±4	79 ±28	28 ±10	93 ±47
Scenario 2 ($\Delta^{14}C_{initial} = -150$ ‰)						
Sea Ice Zone	-	-150	0	0	-	0
Inside Polynya	300	-135	8 ±4	54 ±25	36 ±17	49 ±33
Near Ice Shelf	150	-140	5 ±4	18 ±13	55 ±39	11 ±11

5. SUMMARY AND CONCLUSION

In this study, I have presented the distribution of dissolved inorganic radiocarbon in the Amundsen Sea. Focusing on the inorganic carbon cycling based on carbon isotopes, the main findings are summarized in the following:

- In the upper 300 m layers, average $\Delta^{14}C$ value in the polynya (−135 ‰) was considerably higher than that in the SIZ (−150 ‰).
- $\Delta^{14}C$ value of WW end-member was −147 ‰.
- $\Delta^{14}C$ values in the deep layer were much lower (average of −158 ‰), confirming that CDW was the major source.
- Biogeochemical processes such as GMW input, benthic efflux and remineralization of sinking organic particles contributed negligible amount of carbon to the DIC budget to change the radiocarbon signature in the water column.
- Air-sea exchange is the primary process to increase $\Delta^{14}C$ signature in the upper layer.
- Based on calculated CO_2 exchange rates, the initial radiocarbon distribution was suggested to lie closer to the radiocarbon

distribution of SIZ, implying longer residence time in the upper layer than one year.

This study provides an initial set of data to understand the inorganic carbon cycling in this climate-sensitive region. Warming climate may change the characteristics of the Amundsen Sea more like the polynya rather than sea-ice zone. How the Amundsen Sea will respond to the changing climate in terms of atmospheric CO_2 uptake is unknown. Better characterization of the biological carbon pump operating in the Amundsen Sea adopting various methods including radiocarbon measurements of carbon reservoirs will be necessary.

6. REFERENCES

Arrigo, K.R. and van Dijken, G.L. (2003) Phytoplankton dynamics within 37 Antarctic coastal polynya systems. *Journal of Geophysical Research* 108 (C10), 3271, doi:10.1029/2002JC001739

Arrigo, K. R., van Dijken, G. and Long, M. (2008) Coastal Southern Ocean: A strong anthropogenic CO_2 sink. *Geophysical Research Letters* 35(21). doi:10.1029/2008gl035624

Arrigo, K.R., Lowry, K.E. and van Dijken, G.L. (2012). Annual changes in sea ice and phytoplankton in polynyas of the Amundsen Sea, Antarctica. *Deep Sea Research II* 71-76: 5-15. doi:10.1016/j.dsr2.2012.03.006

Bates, N.R. (2006) Air-sea CO_2 fluxes and the continental shelf pump of carbon in the Chukchi Sea adjacent to the Arctic Ocean. *Journal of Geophysical Research* 111 (C10013).

Bauer, J.E., Druffel, E.R.M, Wolgast, D.M., Griffin, S. and Masiello, C.A. (1998) Disstributions of dissolved organic and inorganic carbon and radiocarbon in the eastern North Pacific continental margin. *Deep Sea Research II* 45: 689-713

Bertrand, C., Walker, B., Griffin, S. and Druffel, E.R.M. (2013) Comparison

of particulate organic and dissolved inorganic radiocarbon signatures in the surface northeast Pacific Ocean. *Radiocarbon* (55): 1651-1658

Broecker, W.S. and Peng, T.-H. (1982) *Tracers in the Sea*, Lamont-Doherty Earth Observatory, Columbia University, Palisades, N.Y.

Dickson, A.G., Sabine, C.L. and Christian, J.R. (2007) *Guide to Best Practices for Ocean CO_2 Measurements*. PICES Special Publication 3, 191 pp.

Druffel, E.R.M., Bauer, J.E., Griffin, S., Beaupré, S.R. and Hwang, J. (2008) Dissolved inorganic radiocarbon in the North Pacific Ocean and Sargasso Sea. *Deep Sea Research I* 55(4): 451-459. doi:10.1016/j.dsr.2007.12.007

Druffel., E.R.M. and Griffin, S. (2008) Daily variability of dissolved inorganic radiocarbon at three sites in the surface ocean. *Marine Chemistry* 110: 185-189

Ducklow, H.W., Wilson, S.E., Post, A.F., Stammerjohn, S.E., Erickson, M., Lee, S., . . . and Yager, P.L. (2015) Particle flux on the continental shelf in the Amundsen Sea Polynya and Western Antarctic Peninsula. *Elementa: Science of the Anthropocene* 3. 000046. doi:10.12952/journal.elementa.000046

Fireman, E.L. and Norris, T.L. (1982) Ages and composition of gas trapped

in Allan Hills and Byrd core ice. *Earth and Planetary Science Letters* 60: 339-350

Fischer, G. (1991) Stable carbon isotope ratios of plankton carbon and sinking organic matter from the Atlantic sector of the southern ocean. *Marine Chemistry* 35: 581-596

Gade, H.G. (1979) Melting of ice in sea water: A primitive model with application to the Antarctic Ice Shelf and icebergs. Journal of Physical Oceanography 9: 189-198

Graven, H.D., Guilderson, T.P. and Keeling, R.F. (2012) Observations of radiocarbon in CO_2 at seven global sampling sites in the Scripps flask network: Analysis of spatial gradients and seasonal cycles, *Journal of Geophysical Research* 117.

Griffith, D.R., McNichol, A.P., Xu, L., McLaughlin, F.A., Macdonald, R.W., Brown, K.A. and Eglinton, T.I. (2012) Carbon dynamics in the western Arctic Ocean: insights from full-depth carbon isotope profiles of DIC, DOC, and POC. *Biogeosciences* 9:1217-1224

Ha, H.K., Wåhlin, A. K., Kim, T.W., Lee, S.H., Lee, J.H., Lee, H.J., . . . and Kalén, O. (2014) Circulation and modification of warm deep water on the central Amundsen shelf. *Journal of Physical Oceanography* 44(5): 1493-1501. doi:10.1175/jpo-d-13-0240.1

Hahm, D., Rhee, T.S., Kim, H.-C, Park, J, Kim, Y.-N, Shin, H.C. and Lee, S.H. (2014) Spatial and temporal variation of net community production and its regulating factors in the Amundsen Sea, Antartica. *Journal of Geophysical Research*. *Oceans* (119): 2815-2826

Hoppema, M., Stoll, M.H.C. and Baar, H.J.W. (2000) CO_2 in the Weddell Gyre and Antarctic Circumpolar Currenr: austral autumn and early winter. *Marine Chemistry* 72: 203-220

Huppert, H.E. and Josberger, E.G. (1980) The melting of ice in cold stratified water. Journal of Physical Oceanography 10(6): 953–960

Hyun, J.-H., Kim, S.-H., Yang, E.J., Choi, A. and Lee, S. H. (2016). Biomass, production, and control of heterotrophic bacterioplankton during a late phytoplankton bloom in the Amundsen Sea Polynya, Antarctica. *Deep Sea Research II* 123: 102-112. doi:10.1016/j.dsr2.2015.10.001

Jacobs, S. S., Hellmer, H. H. and Jenkins, A. (1996) Antarctic Ice Sheet melting in the southeast Pacific. *Geophysical Research Letters* 23(9): 957-960. doi:10.1029/96gl00723

Jacobs, S.S., Jenkins, A., Giulivi, C.F. and Dutrieux, P. (2011) Stronger ocean circulation and increased melting under Pine Island Glacier ice shelf. *Nature Geoscience* 4: 519-523. doi:10.1038/ngeo1180

Jacobs, S., Jenkins, A., Hellmer, H., Giulivi, C., Nitsche, F., Huber, B. and Guerrero, R. (2012) The Amundsen Sea and the Antarctic Ice Sheet. *Oceanography* 25(3): 154-163. doi:10.5670/oceanog.2012.90

Jenkins, A., Dutrieux, P., Jacobs, S.S., McPhail, S.D., Perrett, J.R., Webb, A.T. and White, D. (2010) Observations beneath Pine Island Glacier in West Antarctica and implications for its retreat. *Nature Geoscience* 3: 468-472. doi:10.1038/ngeo890

Key, R.M. (1996) WOCE Parcific Ocean Radiocarbon Program. *Radiocarbon* 38: 415-423

Key, R., and McNichol, A. (2012) Radiocarbon Measurements in the Indian Ocean aboard RVIB Nathaniel B. Palmer. *Oceanography* 25 (3): 152-153. doi:10.5670/oceanog.2012.89

Kim, B.K., Joo, H., Song, H.J., Yang, E.J., Lee, S. H., Hahm, D., . . . and Lee, S.H. (2014) Large seasonal variation in phytoplankton production in the Amundsen Sea. *Polar Biology* 38: 319-331. doi:10.1007/s00300-014-1588-5

Kim, I., Hahm, D., Rhee, T.S., Kim, T.W., Kim, C.-S. and Lee, S. (2016) The distribution of glacial meltwater in the Amundsen Sea, Antarctica, revealed by dissolved helium and neon. *Journal of Geophysical Research. Oceans* 121. doi:10.1002/20015JC011211

Kim, M., Hwang, J., Kim, H.J., Kim, D., Yang, E.J., Ducklow, H.W., . . . and Lee, S. (2015) Sinking particle flux in the sea ice zone of the Amundsen Shelf, Antarctica. *Deep Sea Research I* 101: 110-117.

Kim, S.-H., Choi, A., Yang, E.J., Lee, S.H. and Hyun, J.-H (2016) Low benthic respiration and nutrient flux at the highly productive Amundsen Sea Polynya, Antarctica. Deep Sea Research II 123: 92-101. doi:10.1016/j.dsr2.2015.10.004

Leboucher, V., Orr, J., Jean-Baptiste, P., Arnold, M., Monfray, P., Tisnerate-Lorde, N., Poisson, A. and Duplessy, J.-C. (1999) Oceanic radiocarbon between Antarctica and South Africa along WOCE section I6 at 30 °E. *Radiocarbon* 41: 51-73

Libby, W. F. (1952) *Radiocarbon Dating*. University of Chicago Press, 218-222.

Mackensen, A. (2001) Oxygen and carbon stable isotope tracers of Weddell Sea water masses: new data and some paleoceanographic implications. *Deep Sea Research I* 48: 1401-1422

Matsumoto, K. (2007) Radiocarbon-based circulation age of the world oceans. *Journal of Geophysical Research,* 112 (C9). doi:10.1029/2007jc004095

McNichol, A.P., Jones, G.A., Hutton, D.L. and Gagnon, A.R. (1994) The

rapid preparation of seawater CO2 for radiocarbon analysis at the National Ocean Sciences AMS Facility. *Radiocarbon* 36 (2): 237-246

McNichol, A.P., Osborne, E.A., Gagnon, A.R., Fry, B. and Jones, G.A. (1994) TIC, TOC, DIC, DOC, PIC, POC – unique aspects in the preparation of oceanographic samples for ^{14}C-AMS. *Nuclear Instruments and Methods in Physics Research B* 92: 162-165

Miles, T., Lee, S.H., Wåhlin, A.K., Ha, H.K., Kim, T.W., Assmann, K.M. and Schofield, O. (2015) Glider observations of Dotson Ice Shelf outflow. *Deep Sea Research II*. http://dx.doi.org/10.1016/j.dsr2.2015.08.008i

Mu, L., Stammerjohn, S.E., Lowry, K.E. and Yager, P.L. (2014) Spatial variability of surface pCO2 and air-sea CO_2 flux in the Amundsen Sea Polynya, Antarctica. *Elementa: Science of the Anthropocene*, 2, 000036. doi:10.12952/journal.elementa.000036

Pritchard, H. D., Ligtenberg, S. R., Fricker, H. A., Vaughan, D. G., van den Broeke, M. R. and Padman, L. (2012). Antarctic ice-sheet loss driven by basal melting of ice shelves. *Nature*, 484(7395): 502-505. doi:10.1038/nature10968

Randall-Goodwin, E., Meredith, M.P., Jenkins, A., Yager, P.L., Sherrell,

R.M., Abrahamsen, E. P., . . . and Stammerjohn, S.E. (2015) Freshwater distributions and water mass structure in the Amundsen Sea Polynya region, Antarctica. *Elementa: Science of the Anthropocene*, 3, 000065. doi:10.12952/journal.elementa.000065

Rau, G.H., Takahashi, T. and Des Marais, D.J. (1989) Latitudinal variations in plankton $\delta^{13}C$: implications for CO_2 and productivity in past oceans. *Nature* 341: 516-518Sarmiento, J.L. and Gruber, N. (2006) *Ocean Biogeochemical Dynamics*. Princeton University Press.

Smethie, W.M., Ostlund, H.G. and Loosi, H.H. (1986) Ventilation of the deep Greenland and Norwegian seas: evidence from krypton-85, tritium, carbon-14 and argon-39. *Deep Sea Research* (33): 675-703

Stammerjohn, S., Massom, R., Rind, D. and Martinson, D. (2012) Regions of rapid sea ice change: An inter-hemispheric seasonal comparison. *Geophysical Research Letter* 39. doi:10.1029/2012GL050874

Stuiver, M. and Polach, H.A. (1977) Discussion: reporting of ^{14}C data. Radiocarbon 19: 355-36

Stuiver, M., Quay, P.D. and Őstlund, H.G. (1983) Abyssal water carbon-14 distribution and the age of the world oceans. *Science* 219 (4586): 849-851

Takahashi, T., Sutherland, S.C.,Wanninkhof, R., Sweeney, C., Feely, R.A.,

Chipman, D.W., Hales, B., Friederich, G., Chavez, F. and Sabine, C. (2009) Climatological mean and decadal change in surface ocean pCO_2, and net sea–air CO_2 flux over the global oceans. *Deep Sea Research II* 56(8–10): 554–577.

Tortell, P.D., Long, M.C., Payne, C.D., Alderkamp, A.-C., Dutrieux, P. and Arrigo, K. R. (2012) Spatial distribution of pCO2, ΔO2/Ar and dimethylsulfide (DMS) in polynya waters and the sea ice zone of the Amundsen Sea, Antarctica. Deep Sea Research Part II 71-76:77-93. doi:10.1016/j.dsr2.2012.03.010

Wåhlin, A.K., Yuan, X., Björk, G. and Nohr, C. (2010) Inflow of warm circumpolar deep water in the central Amundsen shelf. Journal of Physical Oceanography 40(6): 1427-1434. doi:10.1175/2010jpo4431.1

Walker, D.P., Brandon, M.A., Jenkins, A., Allen, J.T., Dowdeswell, J.A. and Evans, J. (2007) Oceanic heat transport onto the Amundsen Sea shelf through a submarine glacial trough. *Geophysical Research Letters* 34(2). doi:10.1029/2006gl028154

Wang, X., Yang, G.-P., López, D., Ferreyra, G., Lemarchand, K. and Xie, H. (2009) Late autumn to spring changes in the inorganic and organic carbon dissolved in the water column at Scholaert Channel, West

Antarctica. *Antarctic Science* 22 (2), 145-156 doi:10.1017/s0954102009990666

Weiss, R.H., Őstlund, H.G. and Craig, H. (1979) Geochemical studies in the Weddell Sea. *Deep Sea Research* (26A): 1093-1120

Yager, P.L., Wallace, D.W.R., Johnson, K.M, Smith Jr., W.O., Minnett, P.J. and Deming, J.W. (1995) The northeast water polynya as an atmospheric CO_2 sink: a seasonal rectification hypothesis. *Journal of Geophysical Research* 100 (C3): 4389-4398

Yager, P., Sherrell, R., Stammerjohn, S., Alderkamp, A.-C., Schofield, O., Abrahamsen, P., . . . and Wilson, S. (2012). ASPIRE: The Amundsen Sea Polynya International Research Expedition. *Oceanography* 25(3): 40-53. doi:10.5670/oceanog.2012.73

ABSTRACT (IN KOREAN)

남극 아문젠해는 해빙과 빙붕 용융에 있어 급격한 변화를 겪고 있다. 이 해역에는 남극에서 가장 생산성이 높은 아문젠해 폴리냐가 위치한다. 그러나 아문젠해 폴리냐의 무기 탄소순환에 대한 연구는 극히 드물다. 본 연구에서 저는 아문젠해 내 해양학적으로 다른 세 지역 (해빙역, 아문제해 폴리냐 안 그리고 Dotson 빙붕 근처)에 대한 용존무기탄소의 방사성탄소 분포를 조사하였다. 상부 300 m 층에서 $\Delta^{14}C$ 평균값은 해빙역 (−150 ‰)보다 폴리냐 (−135 ‰)에서 훨씬 높았다. Winter Water의 $\Delta^{14}C$ 값은 −147 ‰이었다. 각 정점 해저면 근처의 $\Delta^{14}C$ 값은 남극 순환심층수의 값에 근접함으로써 심층 내 들어오는 수괴를 반영하였다. 빙붕에서 녹아 공급된 물, 해저면 공급 그리고 수층 내 침강유기입자의 분해 등은 용존무기탄소의 방사성탄소 값을 크게 변화시키지 않았다. 대기−해양 간의 기체 교환이 상층의 방사성탄소 값을 증가시키는데 중점적인 역할을 하였다. 해빙역과 폴리냐 사이 관측된 $\Delta^{14}C$ 값을 토대로 남반구 여름에 폴리냐가 확장되는 동안 대기 이산화탄소의 흡수량을 계산하였다. 본 연구는 기후변화에 민감한 남극 아문젠해 내 무기 탄소순환을 이해하는데 선행적 자료를 제공한다.

주 요 어 : 용존무기탄소, 방사성탄소, 아문젠해, 폴리냐, 대기−해양 간 기체 교환

학 번 : 2014−22420